INTERNATIONAL JOURNAL FOR NUMERICAL METHODS IN FLUIDS, VOL, 26, 533–556 (1998)
Int. J. Numer. Meth. Fluids **26**: 533–556 (1998)

A MIXED FINITE ELEMENT/FINITE VOLUME APPROACH FOR SOLVING BIODEGRADATION TRANSPORT IN GROUNDWATER

CLAUDIO GALLO*,[1] AND GIANMARCO MANZINI

CRS4, Via Nazario Sauro 10, I-09123 Cagliari, Italy

SUMMARY

A numerical model for the simulation of flow and transport of organic compounds undergoing bacterial oxygen- and nitrate-based respiration is presented. General assumptions regarding microbial population, bacteria metabolism and effects of oxygen, nitrogen and nutrient concentration on organic substrate rate of consumption are briefly described. The numerical solution techniques for solving both the flow and the transport are presented. The saturated flow equation is discretized using a high-order mixed finite element scheme, which provides a highly accurate estimation of the velocity field. The transport equation for a sorbing porous medium is approximated using a finite volume scheme enclosing an upwind TVD shock-capturing technique for capturing concentration-unsteady steep fronts. The performance and capabilities of the present approach in a bio-remediation context are assessed by considering a set of test problems. The reliability of the numerical results concerning solution accuracy and the computational efficiency in terms of cost and memory requirements are also estimated. © 1998 John Wiley & Sons, Ltd.

KEY WORDS: mixed finite elements; finite volumes; groundwater flow and transport; biodegradation.

1. INTRODUCTION

The mathematical modelling of a groundwater process is quite complex, involving three important phenomena which take place simultaneously: groundwater flow, transport of different chemical species and microbial biodegradation kinetics. In particular, the last of these turns out to play a very important role in describing realistic situations.

Actually, the importance of microbial activity in degrading organic substances in both subsurface and deep groundwater has been widely recognized in recent years by many authors. For example, see References [1] and [2] in the first case and Reference [3] in the second case. In these works there is some evidence that heterotrophic bacteria grow in colonies and their presence has been positively correlated to plumes of organic substances.

Several modes have also been proposed for monitoring and predicting the dynamics of subsurface pollutant plumes, especially when some remediation strategies are to be planned.

For this purpose, various methodologies have been considered, based on different assumptions. For example, some authors assume the presence of two distinct phases, bulk flow and microbial colonies, interconnected via mass exchange [4–9]. Nevertheless, practical consider-

* Correspondence to: CRS4, Via Nazario Sauro 10, I-09123 Cagliari, Italy.
[1] Email: fender@crs4.it

Contract grant sponsor: Sardinia Regional Authorities

CCC 0271–2091/98/050533–24$17.50

Received July 1996
Revised March 1997

ations have drawn attention to the fact that in several cases the characteristic time of mass exchange between aqueous solution and microbial colonies is much smaller than the characteristic time of concentration variation in bulk flow [10–13]. In the latter case it is not appropriate to distinguish between two different phases in the fluid.

Other authors have also developed models to account for the effects of vegetation in biodegradation of organic compounds. Tracy *et al.* [14,15] presented an unsaturated two-phase 1D flow model coupled with multispecies transport.

Various numerical approaches for solving this class of models are documented in the literature: finite difference technique in 1D [4,5] or 2D [6,11]; optimal test function method [10]; finite elements [7,14,15]; finite elements with modified characteristic method (MMOC), [16] applied by Wood *et al.* [9,13]. Much work has also been devoted to modelling biodegradation kinetics and their parameter calibration [7,9,12,13].

In this context the major issue of the present work is to develop an effective numerical method for solving the saturated flow model coupled with multispecies transport [17] and including biodegradation kinetics, as proposed by Widdowson *et al.* [5]. The saturated flow equations are discretized by a mixed finite element approach [18], while a finite volume technique [19] is applied for solving the transport equations. A shock-capturing technique for sharp concentration fronts is implemented using a TVD (total-variation-diminishing) limiter [20] for solving advection-dominated transport. The biodegradation model was originally developed in 1D by Widdowson *et al.* [5] and has been extended in this work to 2D.

The outline of the paper is as follows. In Section 2 we formulate the governing equations of the model. In Section 3 we present the numerical methods. In Section 4 we present a set of numerical simulations, based on 1D and 2D test cases, to assess the capabilities and performances of the method. Possible realistic applications of the present class of models are also discussed. Finally, in Section 5 we draw some general conclusions and mention the future developments of the current work.

2. MATHEMATICAL MODEL

Three main parts can be identified when modelling biodegradation in groundwater: the flow, the transport and the chemical degradation kinetics. These are based on some leading assumptions that define the level of description and approximation involved.

Each of these parts has been treated separately with a different numerical approach in order to provide a better exploitation of the mathematical nature of the equations involved.

Let us indicate by Ω the spatial domain of computation where the equations are defined. Mathematically, Ω is a simply connected bounded domain in $\mathbb{R}^2$ (in 2D), defined by a closed (1D) surface Γ. Γ can be given as the union of two portions Γ_D and Γ_N where different boundary conditions are imposed, respectively of Dirichlet and Neumann type: $\Gamma = \Gamma_D \cup \Gamma_N$.

2.1. Groundwater flow

The relationship between the pressure p (the total head) and the velocity field $\mathbf{v}$ (the visible effect) in groundwater flow can be expressed as a system of Darcy-type partial differential equations [21]. Under the assumption that the soil matrix is incompressible (soil matrix characteristics—density, texture, specific storage, etc.—are not functions of time, space and pressure itself, as occurs in deformable porous media in which stress, strain and pore fluids are strongly coupled), the saturated flow equations are given as [21]

$$\mathbf{v} = -\mathbf{K}\nabla p, \quad \mathbf{x}\in\Omega, \tag{1}$$

$$-\nabla\cdot\mathbf{v} = S_s\frac{\partial p}{\partial t} - q, \quad (\mathbf{x}, t)\in\Omega\times[0, T], \quad T\geq 0, \tag{2}$$

where $\mathbf{K}(\mathbf{x})$ is the hydraulic conductivity tensor, S_s is the specific storage and q is a source/sink term. Equation (1) relates the vector field $\mathbf{v}$ to the scalar field p via the permeability tensor, which accounts for the soil characteristics. Equation (2) relates the divergence of $\mathbf{v}$ to the product of the time derivative of p and S_s, the specific storage. The specific storage is defined as the volume of water that a unit volume of aquifer releases from storage under a unit decline in hydraulic head [21]: this change in storage for a variation of p is a combined effect of water compressibility (fluid characteristic) and aquifer compaction (variation of solid grain distances). The terms $\mathbf{K}$ and S_s are then the key parameters for describing the groundwater flow.

Equations (1) and (2) are supplemented with a set of boundary conditions for $\mathbf{v}$ and p:

$$p|_{\Gamma_D} = g_D \quad \text{on } \Gamma_D, \tag{3}$$

$$\mathbf{v}\cdot\mathbf{n}\,|_{\Gamma_N} = g_N \quad \text{on } \Gamma_N, \tag{4}$$

using two regular functions g_D and g_N for Dirichlet and Neumann conditions. An appropriate initial solution for p at time $t = 0$ must also be provided.

2.2. Multispecies transport

The transport of a set of interacting chemical species in a saturated porous medium can be modelled using a system of coupled advection–dispersion–reaction equations. The coupling is achieved by means of reaction terms that account for reciprocal chemical interactions. In the model under study we assume that four different species are present [5]: an organic substrate S, dissolved oxygen O, nitrates N and a generic nutrient supply A (e.g. ammonia compounds). The physical quantities referring to these four species will be respectively indicated throughout the paper by the subscripts S, O, N and A. This basic assumption yields the four-PDE system

$$R_S\frac{\partial C_S}{\partial t} = -\nabla\cdot(\mathbf{v}C_S) + \nabla\cdot(\mathbf{D}_S\nabla C_S) + \frac{N_c}{n}\Lambda_S, \tag{5}$$

$$R_O\frac{\partial C_O}{\partial t} = -\nabla\cdot(\mathbf{v}C_O) + \nabla\cdot(\mathbf{D}_O\nabla C_O) + \frac{N_c}{n}\Lambda_O, \tag{6}$$

$$R_N\frac{\partial C_N}{\partial t} = -\nabla\cdot(\mathbf{v}C_N) + \nabla\cdot(\mathbf{D}_N\nabla C_N) + \frac{N_c}{n}\Lambda_N, \tag{7}$$

$$R_A\frac{\partial C_A}{\partial t} = -\nabla\cdot(\mathbf{v}C_A) + \nabla\cdot(\mathbf{D}_A\nabla C_A) + \frac{N_c}{n}\Lambda_A, \tag{8}$$

which describes the variation of the four concentrations C_S, C_O, C_N and C_A with respect to space $\mathbf{x}$ and time t. R_S, R_O, R_N and R_A are the retardation factors (which account for the increased soil capacity due to adsorption of dissolved compounds onto solid grains), $\mathbf{D}_S$, $\mathbf{D}_O$, $\mathbf{D}_N$ and $\mathbf{D}_A$ are the diffusion–dispersion tensors, N_c is the number of bacterial colonies per unit volume, n is the porosity, and Λ_S, Λ_O, Λ_N and Λ_A are the reaction coefficients which enclose the coupling effects between the transport equations. Appropriate boundary conditions such as inlet, outlet and no-flow, and initial solutions must also be provided. These issues will be specified in more detail in Section 4 when we present the test cases.

2.3. Biodegradation kinetics and microbial growth

The model under study is based on the 'microcolony concept' which was originally presented for two species by Molz *et al.* [4] and further extended to four species by Widdowson *et al.* [5]. Subsurface bacteria are thus assumed to reside in microcolonies, which are approximated as small flat patches attached to soil solid grains [4].

Assuming that the reaction process within microcolonies is fast compared with the change in bulk flow concentrations [4], the reaction terms Λ_i can be written explicitly as diffusional mass exchange between the bulk and the colonies, yielding

$$\Lambda_{\mathrm{S}} = D_{\mathrm{Sb}} \frac{C_{\mathrm{S}} - c_{\mathrm{S}}}{\delta} \beta, \tag{9}$$

$$\Lambda_{\mathrm{O}} = D_{\mathrm{Ob}} \frac{C_{\mathrm{O}} - c_{\mathrm{O}}}{\delta} \beta, \tag{10}$$

$$\Lambda_{\mathrm{N}} = D_{\mathrm{Nb}} \frac{C_{\mathrm{N}} - c_{\mathrm{N}}}{\delta} \beta, \tag{11}$$

$$\Lambda_{\mathrm{A}} = D_{\mathrm{Ab}} \frac{C_{\mathrm{A}} - c_{\mathrm{A}}}{\delta} \beta. \tag{12}$$

The term Λ_i takes into account the disappearance of the ith species, with i running through the whole set $i = \mathrm{S}, \mathrm{O}, \mathrm{N}, \mathrm{A}$ in Equations (5)–(8). Equations (9)–(12) involve the following terms: D_{Sb}, D_{Ob}, D_{Nb} and D_{Ab} are the diffusion coefficients in the boundary layer for each species; c_{S}, c_{O}, c_{N} and c_{A} are the concentrations of those species within the microbial colonies; β is the total area of the microbial colony across which the diffusional process takes place; δ is the thickness of the diffusional layer separating the bulk motion and the colony.

S, O, N and A are transported within the bulk flow and enter the microcolonies via a diffusive mass transfer mechanism. Once inside the colonies, these species undergo a set of reactions which can be qualitatively summarized as follows: the organic substrate S is metabolized by heterotrophic bacteria that competitively make usage of oxygen O and/or nitrates N as electron acceptors (see Reference [5] for a detailed discussion on this chemical reaction frame). Microbial growth and metabolism are also quantitatively influenced by the nutrient supply A. Microbial growth and related interaction kinetics are often well represented by Monod-like combined relationships [22]: the consumption rates of S, O, N and A are then expressed as a function of their concentrations within the colonies, i.e c_{S}, c_{O}, c_{N} and c_{A} respectively. The mass transferred per unit time from the bulk to the microbial colonies must be equated to the mass consumed per unit time within the colonies as follows:

$$D_{\mathrm{Sb}}\left[\frac{C_{\mathrm{S}} - c_{\mathrm{S}}}{\delta}\right]\beta = \frac{\mu_{\mathrm{o}}}{Y_{\mathrm{o}}}\left[\frac{c_{\mathrm{S}}}{K_{\mathrm{so}} + c_{\mathrm{S}}}\right]\left[\frac{c_{\mathrm{O}}}{K_{\mathrm{o}} + c_{\mathrm{O}}}\right]\left[\frac{c_{\mathrm{A}}}{K_{\mathrm{ao}} + c_{\mathrm{A}}}\right] + \frac{\mu_{\mathrm{n}}}{Y_{\mathrm{n}}}\left[\frac{c_{\mathrm{S}}}{K_{\mathrm{sn}} + c_{\mathrm{S}}}\right]\left[\frac{c_{\mathrm{N}}}{K_{\mathrm{n}} + c_{\mathrm{N}}}\right]\left[\frac{c_{\mathrm{A}}}{K_{\mathrm{an}} + c_{\mathrm{A}}}\right] I(\mathrm{o}), \tag{13}$$

$$D_{\mathrm{Ob}}\left[\frac{C_{\mathrm{O}} - c_{\mathrm{O}}}{\delta}\right]\beta = \frac{\gamma}{\mu_{\mathrm{o}}}\left[\frac{c_{\mathrm{S}}}{K_{\mathrm{so}} + c_{\mathrm{S}}}\right]\left[\frac{c_{\mathrm{O}}}{K_{\mathrm{o}} + c_{\mathrm{O}}}\right]\left[\frac{c_{\mathrm{A}}}{K_{\mathrm{ao}} + c_{\mathrm{A}}}\right] + \alpha_{\mathrm{o}} k_{\mathrm{o}}\left[\frac{c_{\mathrm{O}}}{K'_{\mathrm{o}} + c_{\mathrm{O}}}\right], \tag{14}$$

$$D_{\mathrm{Nb}}\left[\frac{C_{\mathrm{N}} - c_{\mathrm{N}}}{\delta}\right]\beta = \eta\mu_{\mathrm{n}}\left[\frac{c_{\mathrm{S}}}{K_{\mathrm{sn}} + c_{\mathrm{S}}}\right]\left[\frac{c_{\mathrm{N}}}{K_{\mathrm{n}} + c_{\mathrm{N}}}\right]\left[\frac{c_{\mathrm{A}}}{K_{\mathrm{an}} + c_{\mathrm{A}}}\right] I(\mathrm{o}) + \alpha_{\mathrm{n}} k_{\mathrm{n}}\left[\frac{c_{\mathrm{N}}}{K'_{\mathrm{n}} + c_{\mathrm{N}}}\right] I(\mathrm{o}), \tag{15}$$

$$D_{\mathrm{Ab}}\left[\frac{C_{\mathrm{A}}-c_{\mathrm{A}}}{\delta}\right]\beta=\psi\mu_{\mathrm{o}}\left[\frac{c_{\mathrm{S}}}{K_{\mathrm{so}}+c_{\mathrm{S}}}\right]\left[\frac{c_{\mathrm{O}}}{K_{\mathrm{o}}+c_{\mathrm{O}}}\right]\left[\frac{c_{\mathrm{A}}}{K_{\mathrm{ao}}+c_{\mathrm{A}}}\right]+\epsilon\mu_{\mathrm{n}}\left[\frac{c_{\mathrm{S}}}{K_{\mathrm{sn}}+c_{\mathrm{S}}}\right]\left[\frac{c_{\mathrm{N}}}{K_{\mathrm{n}}+c_{\mathrm{N}}}\right]\left[\frac{c_{\mathrm{A}}}{K_{\mathrm{an}}+c_{\mathrm{A}}}\right]I(\mathrm{o}),\tag{16}$$

where μ_{o} and μ_{n} are the specific growth rates, Y_{o} and Y_{n} are the heterotrophic yield coefficients, γ and η are the coefficients for synthesis of heterotrophic biomass for oxygen and nitrogen, α_{o} and α_{n} are the oxygen and nitrogen use coefficients for maintenance energy of bacteria, ψ and ϵ are the ammonia-nitrogen coefficients for producing biomass under aerobic and anaerobic conditions, K_{so}, K_{o} and K_{ao} are the substrate, oxygen and ammonia-nitrogen saturation constants under aerobic conditions, K_{sn}, K_{n} and K_{an} are the substrate, nitrogen and ammonia-nitrogen saturation constants under anaerobic conditions, K'_{o} and K'_{n} are the oxygen and nitrogen saturation constants, $I(\mathrm{o})=K_{\mathrm{c}}/(K_{\mathrm{c}}+c_{\mathrm{O}})$ is the inibition function of the nitrogen-based respiration, depending on the oxygen concentration within the microbial colonies, c_{O} (see Reference [5] for further details), and K_{c} is the inhibition coefficient.

The closure of the mixed differential–algebraic system requires the kinetics of microbial growth to be specified. The balance between biomass reproduction and decay furnishes the following differential equation for bacterial growth [5]:

$$\frac{1}{N_{\mathrm{c}}}\frac{\partial N_{\mathrm{c}}}{\partial t}=\left(\mu_{\mathrm{o}}\left[\frac{c_{\mathrm{S}}}{K_{\mathrm{so}}+c_{\mathrm{S}}}\right]\left[\frac{c_{\mathrm{O}}}{K_{\mathrm{o}}+c_{\mathrm{O}}}\right]\left[\frac{c_{\mathrm{A}}}{K_{\mathrm{ao}}+c_{\mathrm{A}}}\right]-k_{\mathrm{o}}\right)+\left(\mu_{\mathrm{n}}\left[\frac{c_{\mathrm{S}}}{K_{\mathrm{sn}}+c_{\mathrm{S}}}\right]\left[\frac{c_{\mathrm{N}}}{K_{\mathrm{n}}+c_{\mathrm{N}}}\right]\left[\frac{c_{\mathrm{A}}}{K_{\mathrm{an}}+c_{\mathrm{A}}}\right]-k_{\mathrm{n}}\right)I(\mathrm{o}),\tag{17}$$

where k_{n} and k_{o} are the decay constants that account for bacterial death per unit time. Equation (17) has to be completed by an appropriate initial solution at time $t=0$.

3. NUMERICAL FORMULATION

3.1. Mixed finite element method for Darcy law

The coupled system of Equations (1) and (2) in the hydrostatic pressure p and the velocity field $\mathbf{v}$ has been solved by a mixed finite element approach. In this section we briefly review some basic ideas underlying the numerical method, referring to the literature for a detailed exposition. A weak formulation is formally obtained in a standard way by multiplying Equation (1) by $\mathbf{w}$ and Equation (2) by ϕ. The test functions ϕ and $\mathbf{w}$ will be chosen in the same functional spaces as those to which the unknowns belong. Integrating by parts over the domain of computation, we finally get

$$\int_{\Omega}K^{-1}\mathbf{v}\cdot\mathbf{w}\,\mathrm{d}\Omega-\int_{\Omega}p\nabla\cdot\mathbf{w}\,\mathrm{d}\Omega=-\oint_{\Gamma_{\mathrm{D}}}g_{\mathrm{D}}\mathbf{w}\cdot\mathbf{n}\,\mathrm{d}\Gamma,\tag{18}$$

$$\int_{\Omega}S_{\mathrm{s}}\frac{\partial p}{\partial t}\phi\,\mathrm{d}\Omega+\int_{\Omega}(\nabla\cdot\mathbf{v})\phi\,\mathrm{d}\Omega=\int_{\Omega}q\phi\,\mathrm{d}\Omega.\tag{19}$$

The weak formulation of the problem reads as follows: find $\mathbf{v}$ in $H^1(\Omega,\mathrm{div})$ and p in $L^2(\Omega)$ such that Equations (18) and (19) hold for every $\mathbf{w}$ and ϕ chosen in the same functional spaces respectively. The discrete counterpart of (18) and (19) can be introduced as follows. Let us partition the domain of computation Ω into triangular elements Ω_i. Then consider two finite-dimensional functional spaces for velocity and pressure, which are dense in $H^1(\Omega,\mathrm{div})$

and $L^2(\Omega)$ respectively, where we will seek the approximate solutions. These latter functional spaces are usually chosen such that the restriction of the approximate solutions over any elements is a polynomial. The order of the polynomials must be chosen under some compatibility conditions [18,23]. In this work we considered the $\mathscr{BDM}_1$ space with the set of basis functions $\{\mathbf{w}_m\}$ for $\mathbf{u}$ and the space of $\mathscr{P}_0$ polynomials with the set of basis functions $\{\phi_i\}$ for p. In these spaces we get within each triangle a linear spatial dependence description for the velocity and a piecewise constant representation of the pressure. In the mixed finite element formulation the degrees of freedom of the velocity basis functions are associated with the edges of each triangular cell. They consist of the zeroth- and first-order momentum of the normal velocity; they are twice N_{edges}, the number of edges in the mesh. The ones related to the pressure basis functions are instead associated with the cell itself and their number is equal to N_{cells}, the number of cells in the mesh. For more details about the implementation we refer to the Appendix. The discretization of Equations (1) and (2) is thus given by substituting the expressions for $\mathbf{v}$ and p written as linear combinations of $\{\mathbf{w}_j\}$ and $\{\phi_j\}$ respectively:

$$p = \sum_{j=1}^{N_{\text{cells}}} p_j \phi_j, \qquad \mathbf{v} = \sum_{j=1}^{2N_{\text{edges}}} u_j \mathbf{w}_j. \tag{20}$$

After some manipulations we get

$$\sum_{j=1}^{2N_{\text{edges}}} u_j \int_\Omega K^{-1}\mathbf{w}_j \cdot \mathbf{w}_i \, \mathrm{d}\Omega - \sum_{k=1}^{N_{\text{cells}}} p_k \int_\Omega \nabla \cdot w_i \phi_k \, \mathrm{d}\Omega = -\oint_\Gamma g_D \mathbf{w}_i \cdot \mathbf{n}_i \, \mathrm{d}\Omega, \quad i = 1, \ldots, 2N_{\text{edges}}, \tag{21}$$

$$\sum_{j=1}^{2N_{\text{edges}}} u_j \int_\Omega \nabla \cdot \mathbf{w}_j \phi_i \, \mathrm{d}\Omega + \sum_{k=1}^{N_{\text{cells}}} \frac{\Delta p_k}{\Delta t} \int_\Omega S_s \phi_i \phi_k \, \mathrm{d}\Omega - \int_\Omega q \phi_i \, \mathrm{d}\Omega = 0, \quad i = 1, \ldots, N_{\text{cells}}. \tag{22}$$

Here $\mathbf{u} = \{u_i\}$ and $\mathbf{p} = \{p_i^{n+1}\}$ are the ith discrete unknowns associated with velocity and pressure. The delta term $\Delta p_i = p_i^{n+1} - p_i^n$ comes from an explicit backward Euler discretization of the time derivative $\partial p / \partial t$ in Equation (1). Equations (21) and (22) can be rewritten in a more compact form as a system of linear equations

$$\begin{pmatrix} A & -B \\ B^{\mathrm{T}} & D \end{pmatrix} \begin{pmatrix} \mathbf{u} \\ \mathbf{p} \end{pmatrix} = \begin{pmatrix} g_1 \\ g_2 \end{pmatrix}, \tag{23}$$

with the definitions

$$A \equiv (a_{ij}) = \int_\Omega K^{-1}\mathbf{w}_i \cdot \mathbf{w}_j \, \mathrm{d}\Omega, \tag{24}$$

$$B \equiv (b_{ij}) = \int_\Omega \nabla \cdot \mathbf{w}_i \phi_j \, \mathrm{d}\Omega, \tag{25}$$

$$D \equiv (d_{ij}) = \frac{1}{\Delta t} \int_\Omega S_s \phi_i \phi_j \, \mathrm{d}\Omega, \tag{26}$$

$$g_1 \equiv -\oint_\Gamma g_D \mathbf{w}_i \cdot \mathbf{n} \, \mathrm{d}\Gamma, \tag{27}$$

$$g_2 \equiv \int_\Omega q \phi_i \, \mathrm{d}\Omega + \frac{p^n}{\Delta t} \int_\Omega S_s \phi_i \phi_j \, \mathrm{d}\Omega. \tag{28}$$

The simple block structure of (23) suggest applying a Schur decomposition [24] approach, which reduces the problem to the solution of a symmetric positive definite linear system with

a smaller number of degrees of freedom [25]. Let us compute the unknown vector $\mathbf{p}$ from the second equation of system (23):

$$\mathbf{p} = D^{-1}(g_2 - B^{\mathrm{T}}\mathbf{u}). \tag{29}$$

Substituting this in the first equation, we obtain the final linear system

$$(A + BD^{-1}B^{\mathrm{T}})\mathbf{u} = g_1 + BD^{-1}g_2. \tag{30}$$

This system is well-conditioned if the term Δt that appears in the expression for D is sufficiently small, but becomes an ill-conditioned linear problem in the limit $\Delta t \to \infty$, i.e. in the stationary (elliptic) situation. In the latter case the use of an evolutionary formulation for computing the stationary solution results in a very expensive and inefficient approach and special numerical methods should be devised; see e.g. Reference [25] for a more detailed discussion. The present evolutionary formulation has been considered as the basis of the present work, since we are ultimately interested in developing a fully coupled model in which velocity, pressure and concentrations evolve simultaneously in time. Nevertheless, in this paper we present the results of the first stage of this long-term project, in which we focus our attention mainly on the transport properties of the model, since the hypothesis of a saturated soil allows us to completely decouple Equations (1) and (2) from Equations (5)–(8), using in the latter ones the stationary solution of the first ones. Thus all the test cases presented in Section 4 make use of a steady groundwater flow, computed by solving (23) for a very large Δt only once at the beginning of each transport simulation.

3.2. Finite volume approach for transport equations

The solution procedure of Equations (1) and (2) provides a velocity field which satisfies the condition $\nabla \cdot \mathbf{v} = 0$ in the absence of source terms. The 2D advection–dispersion–reaction system (5)–(8) then takes the conservative form

$$\frac{\partial C_i}{\partial t} + \nabla \cdot (\mathbf{f}_i - \mathbf{g}_i) = Q_i, \quad i = \mathrm{S, O, N, A}, \tag{31}$$

where we have introduced the two vector flux functions $\mathbf{f}_i = (v_x C_i, v_y C_i)$ and $\mathbf{g}_i = \mathscr{D}(\mathbf{v})\nabla C_i$, respectively responsible for the advection and dispersion phenomena. $\mathscr{D}(\mathbf{v})$ is a velocity-dependent dispersion tensor given by

$$\mathscr{D} = \alpha_{\mathrm{M}} I + \frac{\alpha_{\mathrm{T}}}{|\mathbf{v}|}\begin{pmatrix} v_x^2 & v_x v_y \\ v_x v_y & v_y^2 \end{pmatrix} + \frac{\alpha_{\mathrm{L}}}{|\mathbf{v}|}\begin{pmatrix} v_y^2 & -v_x v_y \\ -v_x v_y & v_x^2 \end{pmatrix}, \tag{32}$$

where α_{M} is the molecular diffusivity, α_{T} and α_{L} are the transversal and longitudinal dispersivities and I is the unit matrix. The right-hand-side source term Q takes into account the kinetics of biodegradation reaction processes, whose numerical treatment will be presented in the next subsection. Integrating each equation in system (31) over each cell Ω_k of the unstructured triangle-based mesh introduced in the previous subsection, and applying the Gauss theorem, we get the conservative integral formulation

$$\frac{\mathrm{d}}{\mathrm{d}t}\int_{\Omega k} C_i \,\mathrm{d}\Omega + \sum_{j=1}^{3}\int_{e_{j,k}} (\mathbf{f}_i - \mathbf{g}_i)\cdot \mathbf{n}_j \,\mathrm{d}\sigma = \int_{\Omega_k} Q_i \,\mathrm{d}\Omega, \quad k = 1, \ldots, N_{\mathrm{cells}}, \quad i = \mathrm{S, O, N, A}, \tag{33}$$

where $\mathbf{n}_j$ represents the outward unit normal to $e_{j,k}$ the jth edge of the kth triangle Ω_k, and the index i runs as usual over all the species, $i = \mathrm{S, O, N, A}$. This formulation is completely

equivalent to the differential one and its characteristic is that the evolution in time of the total amount of a conserved quantity within any cell Ω_k depends only upon the distribution of the total flux function on the boundary $\partial\Omega_k$. The problem of the evolution of C_i over Ω_k is reduced to the determination of the balance of fluxes on the contour of the domain of interest. Equations (33) advance in time the total amount of the unknowns C_i, which is logically related to the centroid of each computational cell. These equations can be directly discretized in a method-of-lines approach, where the spatial and time derivatives are considered independently. Neglecting for the sake of simplicity the source term, the finite volume approximation of Equations (33) is given by

$$\left.\frac{\mathrm{d}\bar{C}_i}{\mathrm{d}t}\right|_{\Omega_k} = -\sum_{j=1}^{3}\frac{\Delta l_j}{|\Omega_k|}\bar{h}_j(\bar{C}_i^n), \quad k=1,\ldots,N_{\text{cells}}, \quad i=\text{S, O, N, A}, \tag{34}$$

for each computational cell Ω_k, $k=1,\ldots,N_{\text{cells,}}$ whose area is indicated by the symbol $|\Omega_k|$, with Δl_j the length of the jth edge. The term $\bar{h}_j = \mathbf{h}_j \cdot n_j$ is usually referred to as the numerical flux function and discretizes the term $\mathbf{h}|_j = \mathbf{f}|_j - \mathbf{g}|_j$. We remark that Equation (34) evolves in time the set of quantities $\bar{C}_i$ that are the cell averages of the ith conservative variable C_i. The numerical flux function can be regarded as being composed of two different terms, $\bar{h}_j = \bar{h}_j^{\text{adv}} + \bar{h}_j^{\text{disp}}$, that discretize respectively the advective flux $\mathbf{f}|_j$ and the dispersive flux $-\mathbf{g}|_j$. The advective part of the numerical flux, $\bar{h}_j^{\text{adv}}$, is thus calculated via a standard upwind technique, which has been selected because of its high numerical stability:

$$\bar{h}_i^{\text{adv}}|_j = \frac{1}{2}[f_j(C_i^{\text{R}}) + f_j(C_i^{\text{L}})] - \frac{1}{2}|\mathbf{v}_j \cdot \mathbf{n}_j|(C_i^{\text{R}} - C_i^{\text{L}}). \tag{35}$$

In Equation (35), C_i^{R} and C_i^{L} indicate the right- and left-state ith concentration species given by a special reconstruction procedure inside cells. This step provides a double estimate of the pointwise values for each C_i at any cell interface. The second-derivative terms in the flux function g_i are discretized in the numerical flux $\bar{h}_j^{\text{disp}}$ via a central differentiation algorithm. Finally, an explicit two-stage second-order Runge–Kutta time-advancing scheme has been adopted for discretizing $\mathrm{d}C_i/\mathrm{d}t|_{\Omega_k}$. Since the estimation of numerical fluxes requires the knowledge of pointwise values, a special second-order TVD reconstruction has been considered (Figure 1). The reconstruction defines a spatial representation of each species $C_i(\mathbf{x}, t^n)|_{\Omega_k}$ over each computational cell Ω_k. The simplest reconstruction is obviously given by a piecewise constant distribution. The value of $C_i(\cdot, t^n)|_{\Omega_k}$ in the cell Ω_k is assumed in this case to be a constant, equal to $C_i^n|_{\Omega_k}$. In general, one can devise a polynomial reconstruction in space of an arbitrary order, building a high-order-accurate interpolant of a piecewise smooth function from its cell averages. This polynomial is built by a non-linearly stable interpolation of the discrete set of cell-averaged data in order to avoid the appearance of typical order $O(1)$ oscillations, known as the Gibbs phenomenon, at discontinuities. In this way, C_i and its derivatives are not continuous at the boundary, demanding some sophisticated evaluation of the fluxes. Harten *et al.* [26,27], introduced a class of non-linear schemes which are TVD, a

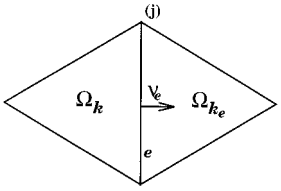

Figure 1. Triangle-based stencil for linear TVD reconstruction

property which ensures that no spurious oscillations are generated, retaining at the same time higher-order (usually second-order) accuracy. For a TVD scheme the total variation of the reconstructed function $R(\cdot\,; C)$ is non-increasing with respect to cell-averaged values:

$$TV(R(\cdot\,;\,\bar{C})) \leq TV(\bar{C}). \tag{36}$$

A standard technique to ensure the TVD property in high-order reconstruction of pointwise values from cell-averaged values consists of introducing an appropriate limiting function. The linear reconstruction is performed species-by-species and for a generic one can also be written in the following way, where we omit for simplicity of notation the species index $i = \mathrm{S, O, N, A}$:

$$C(\mathbf{x}, t) = C(\mathbf{x}_k, t) + (\mathbf{x}_k - \mathbf{x}) \cdot \nabla C|_{\Omega_k}. \tag{37}$$

In Equation (37), $\mathbf{x}_k$ is the centroid of the triangle Ω_k and $C|_{\Omega_k} = C(\mathbf{x}_k, t)$ is the value of the generic species associated with it at time t. An estimate of the gradient $\nabla C|_{\Omega_k}$ inside the cell Ω_k must be provided somehow, which implies an estimate of the two terms $\partial C/\partial x$ and $\partial C/\partial y$. The application of the divergence theorem can easily yield a cell-averaged estimate of these derivatives within the cell, and these values can be taken with second-order accuracy in space as the values at the centroid. The TVD property is directly imposed via a limiting function ψ on the slopes given by the gradient in the reconstruction. Hence the reconstruction takes the final form

$$C(\mathbf{x}, t) = C(\mathbf{x}_k, t) + \psi(\mathbf{x}_k - \mathbf{x}) \cdot \nabla C_k. \tag{38}$$

The limiter ψ takes values in the range 0–1. All the limiters introduced in the literature [28] can be used. However, these limiters are essentially monodimensional. In the present work the truly two-dimensional limiter introduced by Barth [20] has been used, which has shown great reliability and robustness in all the test cases reported in the next section. Some further details are reported in the Appendix.

3.3. Biodegradation and bacterial growth

The solution of Equations (13)–(16) is given by a full Newton–Raphson iteration scheme solved nodally cell-by-cell at the end of each time step:

$$c_i^{k+1,m+1} = c_i^{k+1,m} - [D\mathbf{F}(c_i^{k+1,m}, c_j^{k+1,m})]^{-1}\mathbf{F}(c_i^{k+1,m}, c_j^{k+1,m}), \quad i, j = \mathrm{S, O, N, A}, \tag{39}$$

where k is the time level, m is the current non-linear iteration, $D\mathbf{F}$ indicates the Jacobian matrix and $\mathbf{F}$ is a generic function indicating the left-hand-side minus the right-hand-side terms for any equation in system (13)–(16). The Newton–Raphson scheme has just local convergence, resulting in the requirement that the starting guess iterate be close 'enough' to the final solution. This fact may be a flaw, giving failure of convergence in some situations. For this reason the present scheme was verified separately and was found to be very robust for a large range of parameters and concentration starting values.

Equation (17) is integrated in time using a one-step explicit forward Euler scheme. Bacterial concentration is updated at the end of each time iteration of the transport equations. In the update of Equation (17), numerical stability reasons may sometimes require a time step which is much smaller than the maximum one allowed by the Courant–Friedrichs–Lewy constraint in the solution of the transport equations. Since adopting such a time step for the overall computation would result in a very expensive solution, a fractional multistep integration scheme can be used instead, which reads as

$$N_c^{k+(i+1)\,\Delta t/n_s} = g(N_c^{k+i\,\Delta t/n_s}), \quad i = 0, \ldots, n_s - 1, \tag{40}$$

4. NUMERICAL RESULTS

In this section we present a double set of simulation results obtained on two different benchmark problems. Benchmark test case 1 considers a small-scale simulation of a hypothetical laboratory column experiment like the one proposed by Molz *et al.* [4]. A comparison is shown between the numerical results produced by the present approach and the results given in the literature. Benchmark test case 2 considers realistic field-size simulations of natural and forced remediation from a mild organic substance pollution release. The importance of a reliable flow simulation technique is quite evident in the second case. An erroneous position of the air injection well used in the remediation intervention can almost completely jeopardize its effectiveness.

4.1. Test case 1

The first test case considers a 100 cm long column of porous medium with a given initial concentration and bacterial population distribution. A water solution with a different composition from the initial one feeds the column and transient evolution is simulated up to $t = 4$ days. Changes in bacterial population and biochemistry reactions take place and modify the concentration distribution within the column. The column is approximated with a stripwise 2D rectangular mesh divided into 100 intervals along the axial direction and four intervals along the transversal one, giving a total of 505 nodes and 800 triangular cells. A steady flow field is superimposed with $|v| = 25$ cm day^{-1}. Longitudinal and transversal dispersivities are set to $\alpha_L = \alpha_T = 0.5$ cm for $Pe = 2$ and to $\alpha_L = \alpha_T = 0$ when $Pe \to \infty$ (purely advective case), while α_M was set to zero for both test cases. The time step for the simulation is $\Delta t = 0.02$ days. Table I lists the other parameter values.

The first simulation we performed assumes that the column is filled with water with (i) an initial concentration of 5 mg l^{-1} of both organic substrate and dissolved oxygen and (ii) N and A in excess in order to only account for the interaction substrate–oxygen–bacteria—N and A in such a case are considered non-conditioning factors.

At $t = 0$ days the column is fed by a $C_S = 15$ mg l^{-1} and $C_O = 5$ mg l^{-1} solution, while N and A were still kept in excess.

A second simulation has then been carried out by considering all the species as inert tracers, passively transported along the column.

Figure 2 compares the breakthrough curves obtained by computing the solution with the 1D finite difference method [4] and with the proposed 2D TVD finite volume scheme (restricted to 1D) for $Pe = 2$. The two sets of curves are in good agreement, though some small differences can be noticed. The 2D finite volume scheme appears to be slightly more dissipative than the 1D finite difference one method low Peclet numbers ($Pe = 2$). Some artificial dissipation is in fact produced by the finite volume discretization of the Laplacian terms in the transport equations. Hence a slightly less accurate solution is obtained when the scheme is applied to a regular-structured mesh. This effect apparently depends on a numerical accumulation and propagation of the errors arising in the flux-approximate form of the second-order derivative terms near boundaries. In contrast, when pure advection is present, i.e. $Pe \to \infty$, no Laplacian terms have to be discretized and the 2D finite volume method produces a more accurate approximation of the steep concentration fronts (see Figure 3). In such a case the non-linear

Table I. Biodegradation parameters for test cases 1 (T1) and 2 (T2)

Parameter	R_S	R_O	R_N	R_A	N_c	n	β	δ
Units	—	—	—	—	m^{-3}	—	m^2	m
T1	1.12	1.01	1.0	2.2	1.0×10^{11}	0.3	7.8×10^{-11}	5.0×10^{-4}
T2	1.0	1.0	1.0	1.0	3.53×10^{9}	0.3	3.1×10^{-10}	5.0×10^{-4}
Parameter	D_{Sb}	D_{Ob}	D_{Nb}	D_{Ab}	μ_o	μ_n	Y_o	Y_n
Units	$m^2\ day^{-1}$	$m^2\ day^{-1}$	$m^2\ day^{-1}$	$m^2\ day^{-1}$	—	—	—	—
T1	0.6×10^{-4}	0.71×10^{-4}	1.50×10^{-4}	1.86×10^{-4}	4.34	2.9	0.278	0.5
T2	1.03×10^{-4}	2.19×10^{-4}	1.50×10^{-4}	1.86×10^{-4}	4.34	2.9	0.278	0.5
Parameter	γ	η	α_o	α_n	ψ	ϵ	K_{so}	K_o
Units	—	—	—	—	—	—	$g\ m^{-3}$	$g\ m^{-3}$
T1	1.4	2.2	0.0402	0.10	0.122	0.122	40.0	40.0
T2	1.4	2.2	0.0402	0.10	0.122	0.122	40.0	0.77
Parameter	K_{ao}	K_{sn}	K_n	K_{an}	K'_o	K'_n	K_c	$k_n = k_o$
Units	$g\ m^{-3}$	$g\ m^{-3}$	$g\ m^{-3}$	$g\ m^{-3}$	$g\ m^{-3}$	$g\ m^{-3}$	$g\ m^{-3}$	day^{-1}
T1	1.0	40.0	2.6	1.0	0.77	2.6	1×10^{-4}	0.02
T2	1.0	40.0	2.6	1.0	0.77	2.6	1×10^{-4}	0.02

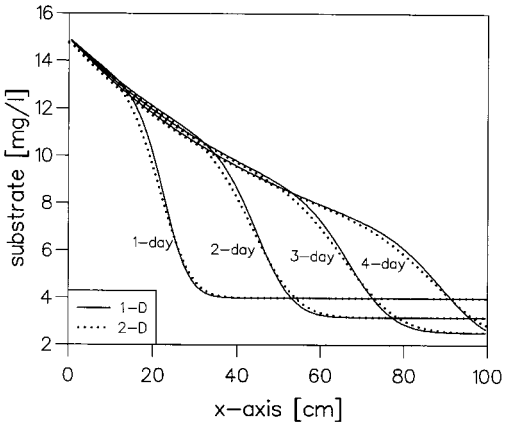

Figure 2. Comparison between monodimensional model and bidimensional model for case $Pe = \infty$

numerical dissipation generated by the TVD-limited reconstruction algorithm, previously discussed, allows one to stabilize the calculation and to resolve the advected front of concentration in a few contiguous cells.

As observed by Widdowson *et al.* [5], biodegradation transport is mainly an advection-dominated phenomenon, where the dissipative contribution coming from Laplacian terms is nearly negligible. In such a case the numerical solution computed with the proposed TVD finite volume method is expected to be very accurate, especially in real field-size simulations. In contrast, when dissipation cannot be neglected with respect to advection, the use of different numerical techniques, e.g. classical finite element methods, should be envisaged [17].

4.2. Test case 2

The second problem considers a zone where a high-concentration plume of organic pollutant (substrate) has been released and industrial fertilizers and concimes (nitrates and nutrients) have been spread. The remediation choice spans between the natural biological reaction of the soil and a human-forced process. In the former case the biodegradation kinetics is simply left to take its course, while in the latter case special substances (e.g. air enriched with oxygen) are

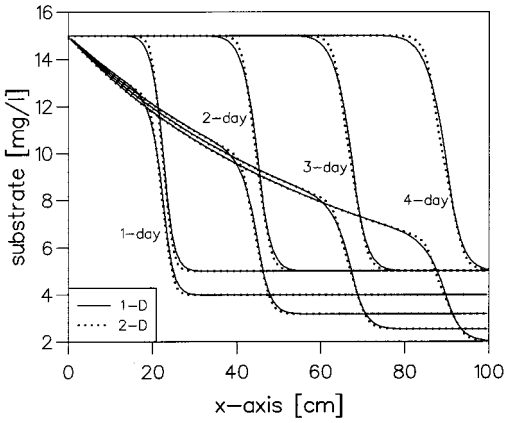

Figure 3. Comparison between the monodimensional model and bidimensional model for case $Pe \to \infty$

injected into the soil to accelerate the process of organic compound degradation. The major issue in this test case is to describe the changes in the concentrations of the four interacting species transported by the water flow field. Three possible scenarios have thus been simulated and results are reported in this subsection: the natural biological reaction process, an oxygen-driven remediation process and, finally, a remediation strategy making use of pumpage to deviate the flow in different patterns.

The region under study has been hypothetically identified with the alluvional plain of Capoterra in Sardinia, Italy. This choice is motivated by the availability of many hydrological and hydrogeological data and some knowledge of the geological conformation of the zone: this fact allows the simulation to be particularly realistic. A snapshot of Sardinia and Capoterra is shown in Figure 4. The white portion identifies the plain. Figure 5 shows a schematic representation of the test case. The approximate location of agricultural settlements, potential sources of organic compounds and nutrient wastes, is indicated. The same picture also illustrates the boundary conditions for the flow and the transport problem.

The soil is assumed to be heterogeneous and isotropic. The geological characteristics allow one to identify three homogeneous subzones, whose boudaries are plotted in Figure 5. These three areas present comparable hydrological parameter values, e.g. hydraulic conductivity, porosity, dispersivity, etc.

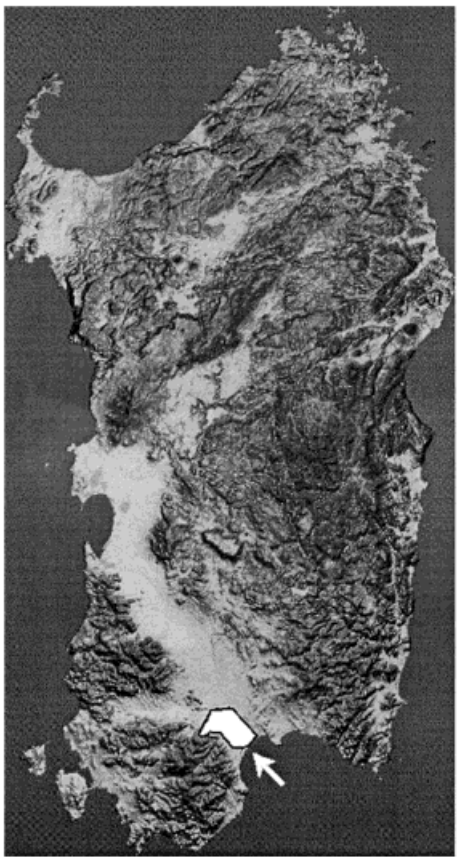

Figure 4. Geographical map of Sardinia

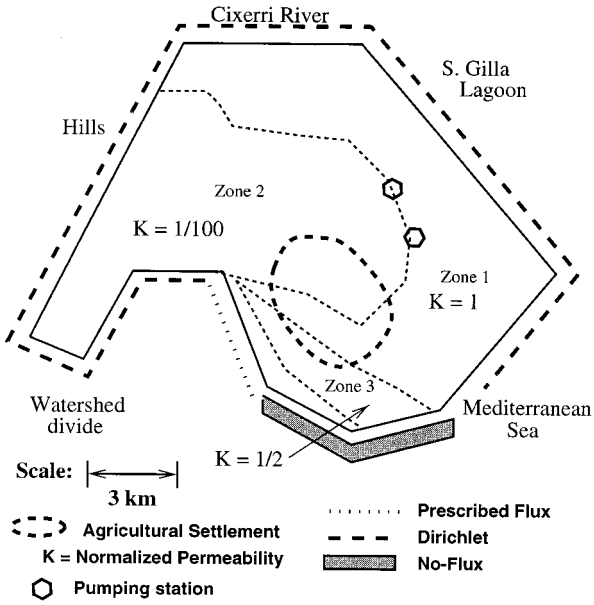

Figure 5. Capoterra's alluvional plain characteristics and boundary conditions

In the agricultural settlements, the initial concentrations of organic substrate (xylene, toluene, etc.) and nitrates and nutrients (industrial fertilizers) are assumed to be 5–30 times those in the surroundings. Initial high-concentration spots are taken only partially overlapping in order to evaluate the effects of the velocity fields on the contaminant plumes. A 20-times-higher concentration of oxygen has been assumed in a spot partially overlapping with the previous ones. Bacterial colonies are assumed to be homogeneously distributed. Table II gives the peak values for the high-concentration spots, while a starting value of 1 mg l^{-1} was set elsewhere in the domain. The simulation period extends up to $t_{max} = 8000$ days. The computational domain is discretized using an unstructured mesh composed of 1033 nodes and 1941 triangular cells (Figure 6). A fixed time step of $\Delta t = 1$ day was used. Flow boundary conditions are provided by field data measurements. A total pressure is imposed and a steady state groundwater flow field is computed, as shown in Figure 7. The values of $|K|$ used for the simulation were 1000, 10 and 500 m day^{-1} for zones 1, 2 and 3 respectively. Soil heterogeneities strongly affect the velocity pattern: preferential paths in high-permeability zones are clearly evident. The velocity modulus in high-permeability regions is several orders of magnitude larger than that in low-permeability

Table II. Peak concentration values for test case 2

Conditions	Time t (years)	S (mg l^{-1})	O (mg l^{-1})	N (mg l^{-1})	A (mg l^{-1})
Low oxygen	0	30	20	10	5
	2.7	15	19.2	7.2	3.9
	13.1	5.8	16.2	4.9	3.1
High oxygen	0	30	200	10	5
	13.1	3.8	173	4.9	3.0
Pumping	0	30	200	10	5
	13.1	7.6	199	5.9	3.7

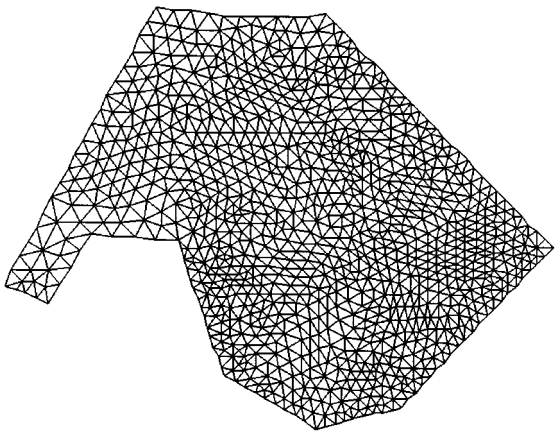

Figure 6. Computational mesh (1033 nodes, 1941 triangular cells)

regions. The transport equations are solved using the flow field computed in the previous step. The values of α_L and α_T were set to 0.1 and 0.1 m, 0.5 and 0.1 m and 0.05 and 0.01 m for zones 1, 2 and 3 respectively, while α_M was set to zero.

Figures 8 and 9 illustrate the initial distribution of the concentration maps for S and O respectively (the distributions for N and A are not shown, since they are quite similar to that of O).

Figures 10 and 11 show the concentration maps for S and O respectively at $t = 2.7$ years in the case of natural bioremediation (note that the legend scale for most of the figures for $t > 0$ has been modified according to the peaks of concentration given in Table II). Since the high-concentration spots are not completely overlapping at the starting time, a small difference in the initial positions of pollutants produces dramatic differences in their distributions after

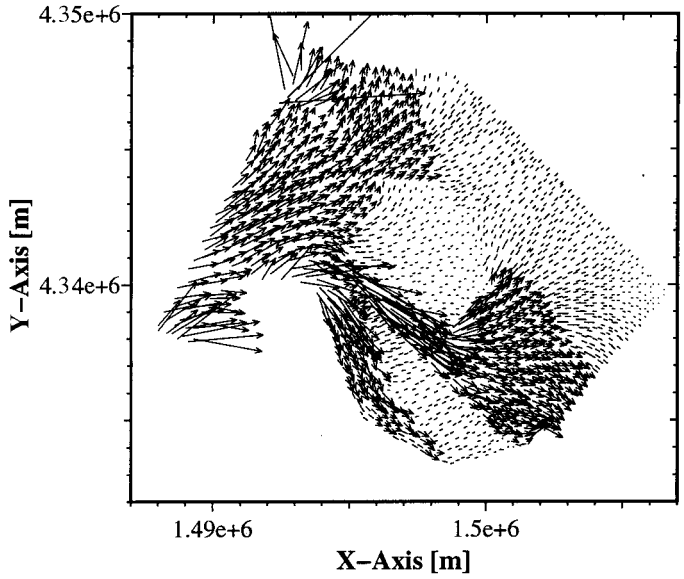

Figure 7. Velocity field with no artificial pumping

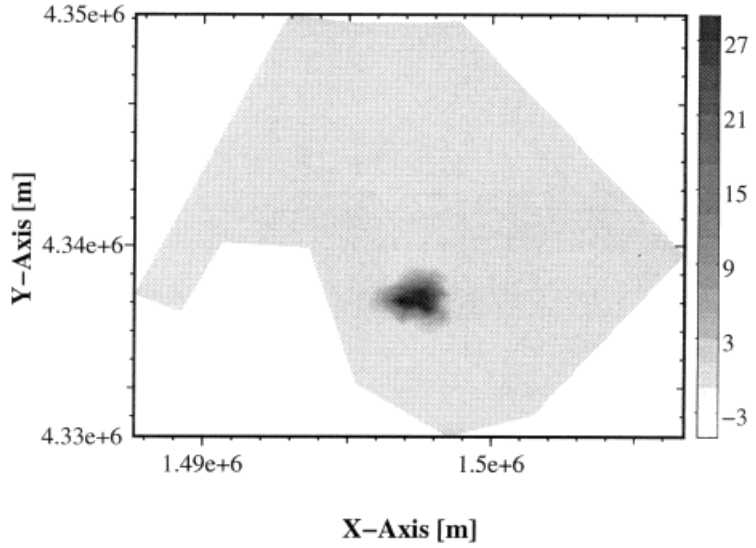

Figure 8. Substrate concentration map for $t = 0$

just 2.7 years. The slow kinetics of the biodegradation process, coupled with the heterogeneous velocity pattern, leaves the oxygen—the most important agent influencing the metabolism of bacteria—almost unused.

Figure 12 shows the spatial distribution of the substrate concentration at $t = 13.1$ years. The major part of the contaminant has disappeared and only small traces are still present. The simulation indicates that a period of approximately 13 years is required for the natural degradation of the major part of the organic substrate.

The same problem has been solved with an increased initial oxygen concentration. The simulation was repeated assuming that in the agricultural settlements the oxygen concentration

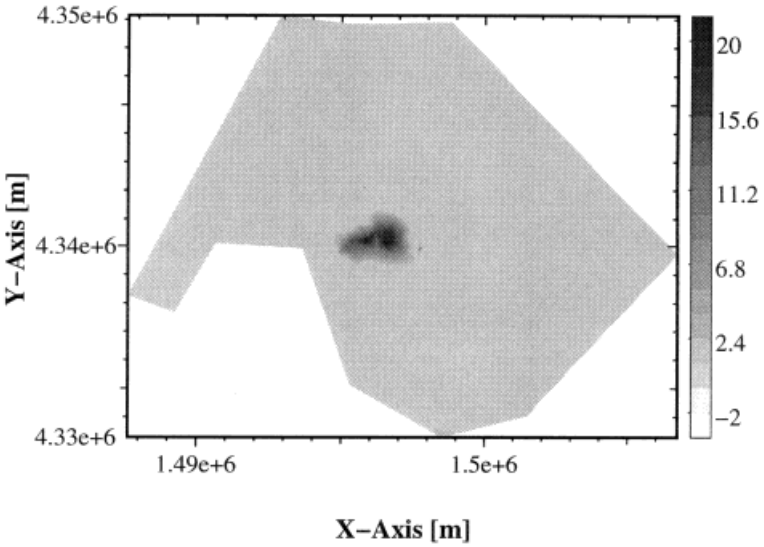

Figure 9. Oxygen concentration map for $t = 0$

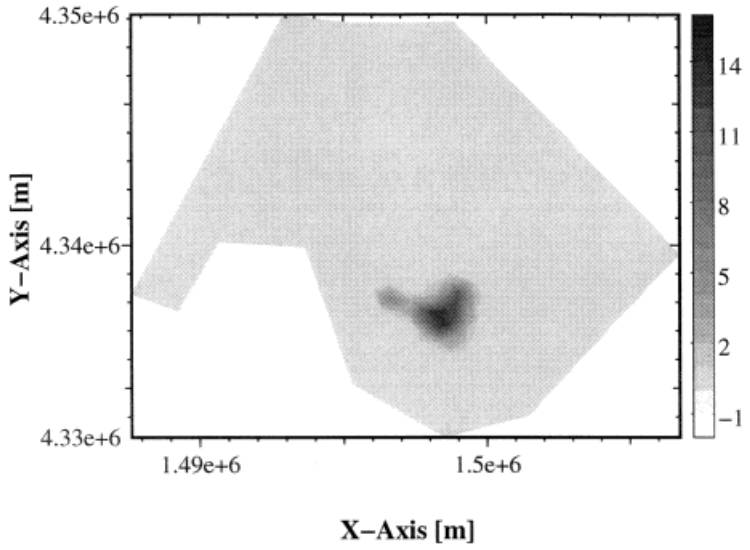

Figure 10. Substrate concentration map for $t = 2.7$ years

is ten times higher than in the first case. The degradation kinetic process is thus accelerated and at $t = 13.1$ years the organic substrate is strongly reduced with respect to the previous result—compare Figures 12 and 13 and refer to Table II for the peak values.

The acceleration in the degradation kinetics also limits in this case the key shortcoming due to the transport driven by the flow pattern. The spatial distributions of nitrates (N) in the first and in the second simulation are almost identical. Hence an increase in the initial concentration of oxygen does not seem to significantly affect the evolution of the nitrates concentration (Table II), at least for the set of reactions considered in the present model. In contrast, nutrients (A) are slightly more consumed in the second simulation.

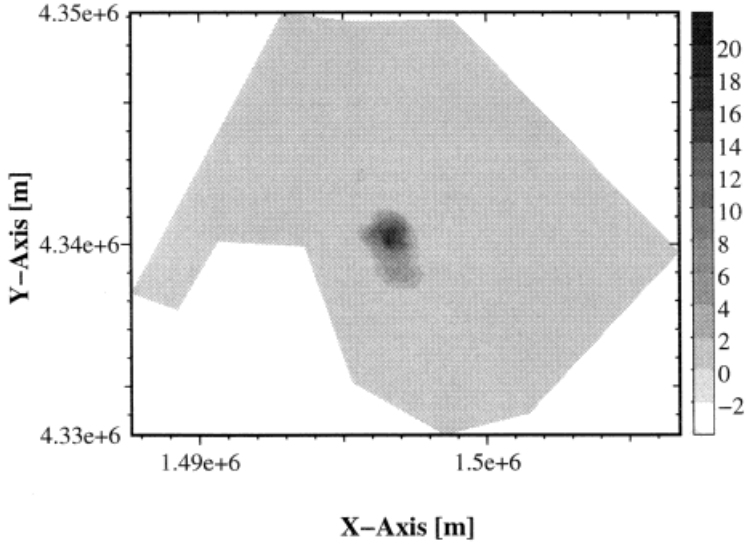

Figure 11. Oxygen concentration map for $t = 2.7$ years

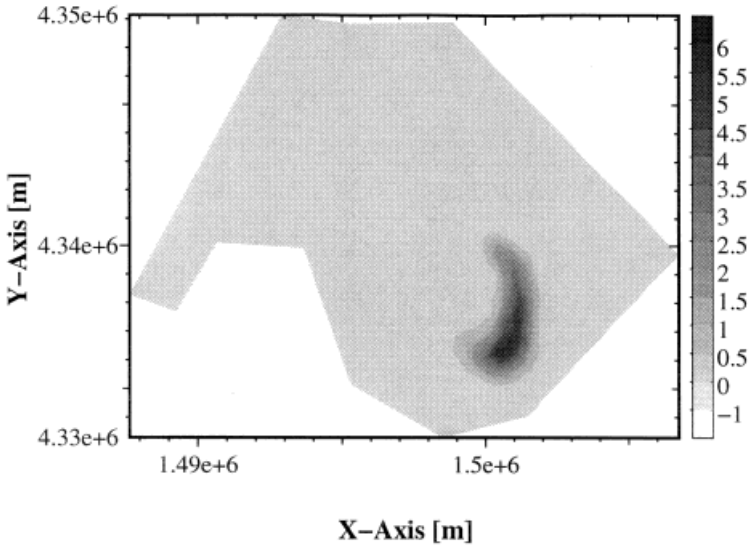

Figure 12. Substrate concentration map for $t = 13.1$ years

A third simulation has then been performed by adding two pumping stations in order to modify the flow pattern, as shown in Figure 14—compare with Figure 7. No substantial variations can be noticed in the species concentrations at $t = 2.7$ years. However, some deviations are evident at $t = 13.1$ years; see Figure 15. It is clearly seen that the concentration distributions are strongly influenced by the pumping-induced flow patterns, although no further decrease in organic substrate concentration is obtained within 13 years of simulation.

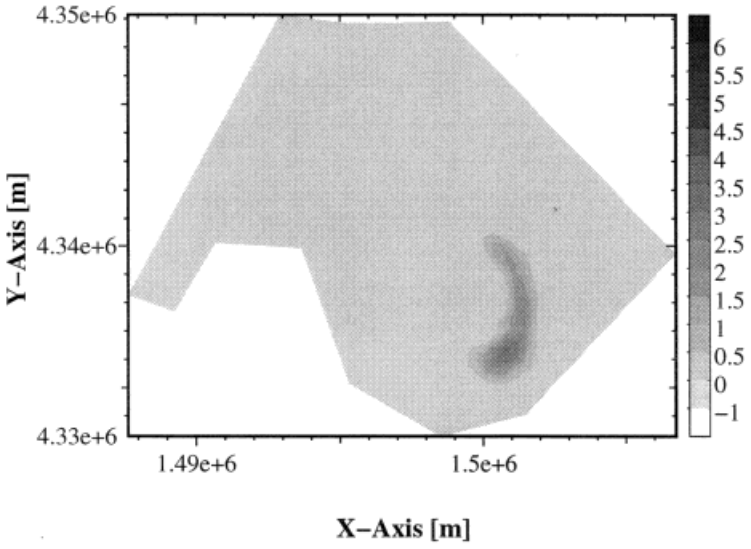

Figure 13. Substrate concentration map for $t = 13.1$ years and increased dissolved oxygen concentration

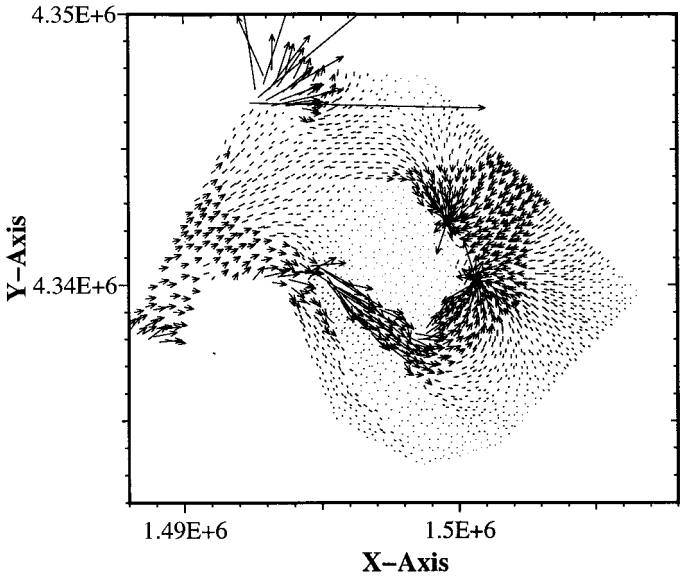

Figure 14. Velocity field for case of artificial pumping

5. FINAL REMARKS

A mixed finite element/finite volume numerical approach for solving flow and transport problems in groundwater had been presented. This approach has been applied to simulate the evolution of organic substrate plumes, metabolized by the heterotrophic micro-organisms present in subsurface saturated aquifers.

Several simulation results have been reported to stress the characteristics of the numerical approach adopted. These results support the robustness of the finite volume formulation for

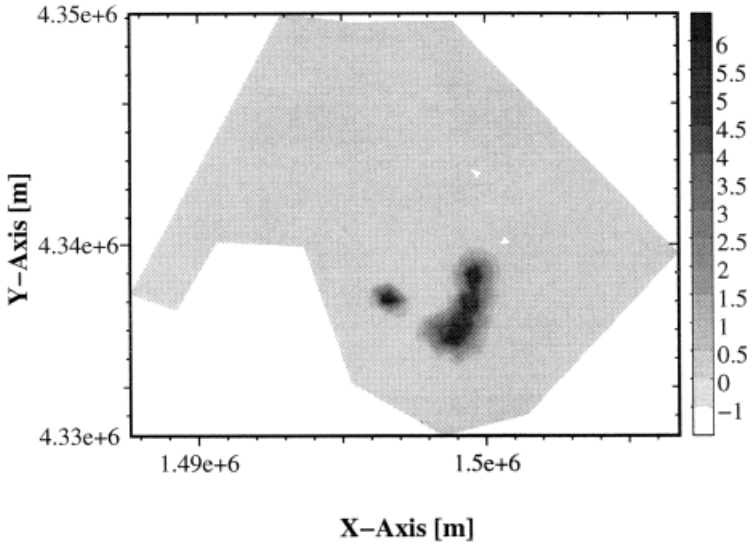

Figure 15. Substrate concentration map for $t = 13.1$ years, increased dissolved oxygen concentration and modified velocity field

solving transport: no oscillations, overshoots or undershoots and no detectable numerical dissipation effects appear in the solutions of the purely advective or advection-dominated cases.

The flow field computed using the mixed finite element technique is directly plugged into the finite volume transport solver, confirming the optimal coupling between these two solution techniques [17]. The mixed finite element method yields a very accurate, though expensive in terms of memory and CPU time [17], approximation of the flow field velocity fluxes, also when strong heterogeneities in the geological structure of the porous medium are present.

The computational costs of the finite volume solver in the simulations so far considered can be measured and possible improvements from the computational effort viewpoint can be considered. A run on about 2000-cell meshes requires approximately 2600 s on an IBM RISC/6000 mod.560 machine. The major sections in our implementation, namely advection–dispersion, reconstruction and chemistry computations, take respectively 22%, 38% and 40% of the total CPU time. Obviously, the advection–dispersion computation cannot be suppressed and a second-order-accurate reconstruction scheme is required to ensure good spatial resolution of steep concentration fronts. Some improvements might be expected with a method alternative to the Newton–Raphson algorithm—such as quasi-Newton schemes or special fixed point iteration techniques—for solving more efficiently the 4×4 non-linear system for each node. Nevertheless, the choice of the Newton–Raphson algorithm for solving the non-linear kinetic system has been successful: the algorithm has been shown to be robust and stable, at least in all the situations considered in the present work.

The present model could be useful as a modelization tool, able to predict the effects of interactions between natural biodegradation phenomena and human soil remediation strategies for polluted soils. The application of this model might be helpful in better understanding the processes related to microbial utilization of nutrients and organic substrate. Nevertheless, laboratory and field measurements possibly available can contribute strongly to a deeper understanding of the interaction between the species and the role of the bacteria in biodegradation and also to the calibration of other model parameters.

ACKNOWLEDGEMENTS

We thank Mariagrazia Sciabica (University of Cagliari) for kindly providing hydrological and hydrogeological data for the Capoterra zone. The authors are grateful to the learned referee for his valuable comments. This work has been supported by Sardinia Regional Authorities.

APPENDIX: IMPLEMENTATION DETAILS

In this appendix we illustrate in more detail some issues related to the implementation of the mixed finite element/finite volume technique.

Basis functions for pressure and velocity on triangles

Let us choose for the pressure the $\mathscr{P}_0$ basis functions $\{\phi_i\}$, $i = 1, \ldots, N_{\text{cells}}$, where

$$\phi_i(\mathbf{x}) = \begin{cases} 1 & \text{if } \mathbf{x} \in \Omega_i, \\ 0 & \text{elsewhere.} \end{cases} \tag{41}$$

The discrete form of the velocity is somewhat more complicated. Within any triangle Ω_k of the mesh the method seeks an approximation of the vector function $\mathbf{v}(x, y)$ of the form

$$\mathbf{v}(x, y) = \begin{pmatrix} ax + by + c \\ dx + ey + f \end{pmatrix}, \tag{42}$$

which requires one to specify the six coefficients (a, b, c, d, e, f), i.e. six degrees of freedom. It is straightforward to decompose $\mathbf{v}(x, y)$ on six independent basis functions $\mathbf{w}_k(x, y)$, $k = 1, \ldots, 6$, which have the same functional dependence of $\mathbf{v}$ on (x, y) as in Equation (42):

$$\mathbf{v} = u_1\mathbf{w}_1 + u_2\mathbf{w}_2 + u_3\mathbf{w}_3 + u_4\mathbf{w}_4 + u_5\mathbf{w}_5 + u_6\mathbf{w}_6, \tag{43}$$

where the six terms $(u_1, u_2, u_3, u_4, u_5, u_6)$ correspond one-to-one to the vector $\mathbf{v}$. We now look for six basis functions with the same form of the vector $\mathbf{v}$ given by Equation (42). We will compute the six coefficients which determine any function $\mathbf{w}_k$, $k = 1, \ldots, 6$, by imposing a constraint on the zeroth- and first-order momentum of the quantity $\mathbf{w} \cdot \mathbf{n}$ over the edges of the triangle in which they are defined. Let us define over a generic edge e_i the two line integrals of the normal component of $\mathbf{w}_j$:

$$\mathscr{I}_{ij}^{(0)} = \int_{e_i} \mathbf{w}_j \cdot n \, \mathrm{d}s, \tag{44}$$

$$\mathscr{I}_{ij}^{(1)} = \int_{e_i} \mathbf{w}_j \cdot ns \, \mathrm{d}s. \tag{45}$$

We can impose two different sets of conditions, namely

$$\mathscr{I}_{ij}^{(0)} = \delta_{ij}, \qquad \mathscr{I}_{ij}^{(1)} = 0, \tag{46}$$

$$\mathscr{I}_{ij}^{(0)} = 0, \qquad \mathscr{I}_{ij}^{(1)} = \delta_{ij}, \tag{47}$$

which give us two different types of basis functions, called respectively $w^{(0)}$ and $w^{(1)}$. In this way, any basis function is associated with a well-defined edge e_i of the mesh and will be indicated by $w_i^{(0)}$ or $w_i^{(1)}$, the index i running through all the edges of the mesh, depending on which integral, $\mathscr{I}^{(0)}$ or $\mathscr{I}^{(1)}$, is equal to one on i. We remark that the support of $w_i^{(0)}$ and $w_i^{(1)}$ is given by the two triangles sharing the edge e_i, i.e. only these two triangles have a set of coefficients (a, b, c, d, e, f) not all simultaneously zero. The velocity unknown $\mathbf{v}$ can now be written as

$$\mathbf{v} = \sum_{i=1}^{N_{\text{sides}}} u_i^{(0)} w_i^{(0)} + u_i^{(1)} w_i^{(1)}, \tag{48}$$

where the summation is over the N_{sides} edges of the mesh. We describe now the algorithm to compute the basis functions for triangles. Let us consider a side $e_i = \mathrm{AB}$ defined by the two nodes A and B with co-ordinates (x_1, y_1) and (x_2, y_2). If $\mathbf{n} = (n_x, n_y)$ are the components of the normal vector, given by

$$n_x = y_2 - y_1, \qquad n_y = -(x_2 - x_1), \tag{49}$$

then the two integrals $\mathscr{I}^{(0)}$ and $\mathscr{I}^{(1)}$ are given by

$$\begin{aligned}
\mathscr{I}^{(0)} &= \int_{\mathrm{A}}^{\mathrm{B}} \mathbf{w} \cdot \mathbf{n} \, \mathrm{d}s = \int_{\mathrm{A}}^{\mathrm{B}} [(ax + by + c)n_x + (dx + ey + f)n_y] \, \mathrm{d}s \\
&= \int_0^1 \{a[x_1 + s(x_2 - x_1)]n_x + b[y_1 + s(y_2 - y_1)]n_x + cn_x \\
&\quad + d[x_1 + s(x_2 - x_1)]n_y + e[y_1 + s(y_2 - y_1)]n_y + fn_y\} \, \mathrm{d}s \\
&= a\left(\frac{x_1 + x_2}{2}\right)n_x + b\left(\frac{y_1 + y_2}{2}\right)n_x + cn_x + d\left(\frac{x_1 + x_2}{2}\right)n_y + e\left(\frac{y_1 + y_2}{2}\right)n_y + fn_y,
\end{aligned} \tag{50}$$

$$\begin{aligned}
\mathscr{I}^{(1)} &= \int_{\mathrm{A}}^{\mathrm{B}} \mathbf{w} \cdot \mathbf{n}s \, \mathrm{d}s = \int_{\mathrm{A}}^{\mathrm{B}} [(ax + by + c)n_x + (dx + ey + f)n_y]s \, \mathrm{d}s \\
&= \int_0^1 \{a[x_1 s + s^2(x_2 - x_1)]n_x + b[y_1 s + s^2(y_2 - y_1)]n_x + cn_x s \\
&\quad + d[x_1 s + s^2(x_2 - x_1)]n_y + e[y_1 s + s^2(y_2 - y_1)]n_y + fn_y s\} \, \mathrm{d}s \\
&= a\left(\frac{x_1 + 2x_2}{6}\right)n_x + b\left(\frac{y_1 + 2y_2}{6}\right)n_x + \frac{1}{2}cn_x + d\left(\frac{x_1 + 2x_2}{6}\right)n_y + e\left(\frac{y_1 + 2y_2}{6}\right)n_y + \frac{1}{2}fn_y.
\end{aligned} \tag{51}$$

For any triangle Ω_k it is now possible to write the six conditions as a system of six linear equations in the unknowns $U=(a, b, c, d, e, f)^{\mathrm{T}}$. The coefficients of the equations are given by the expression of the two integrals $\mathscr{I}^{(0)}$ and $\mathscr{I}^{(1)}$ and form a matrix, say $\mathscr{A}$. The right-hand side is given by the columns of the unity matrix I (one per basis function). For example, for basis function $\mathbf{w}_i^{(0)}$ we have

$$\begin{pmatrix}
\left(\frac{x_1+x_2}{2}\right)n_x^{12} & \left(\frac{y_1+y_2}{2}\right)n_x^{12} & n_x^{12} & \left(\frac{x_1+x_2}{2}\right)n_y^{12} & \left(\frac{y_1+y_2}{2}\right)n_y^{12} & n_y^{12} \\
\left(\frac{x_2+x_3}{2}\right)n_x^{23} & \left(\frac{y_2+y_3}{2}\right)n_x^{23} & n_x^{23} & \left(\frac{x_2+x_3}{2}\right)n_y^{23} & \left(\frac{y_2+y_3}{2}\right)n_y^{23} & n_y^{23} \\
\left(\frac{x_3+x_1}{2}\right)n_x^{31} & \left(\frac{y_3+y_1}{2}\right)n_x^{31} & n_x^{31} & \left(\frac{x_3+x_1}{2}\right)n_y^{31} & \left(\frac{y_3+y_1}{2}\right)n_y^{31} & n_y^{31} \\
\left(\frac{x_1+2x_2}{6}\right)n_x^{12} & \left(\frac{y_1+2y_2}{6}\right)n_x^{12} & \frac{1}{2}n_x^{12} & \left(\frac{x_1+2x_2}{6}\right)n_y^{12} & \left(\frac{y_1+2y_2}{6}\right)n_y^{12} & \frac{1}{2}n_y^{12} \\
\left(\frac{x_2+2x_3}{6}\right)n_x^{23} & \left(\frac{y_2+2y_3}{6}\right)n_x^{23} & \frac{1}{2}n_x^{23} & \left(\frac{x_2+2x_3}{6}\right)n_y^{23} & \left(\frac{y_2+2y_3}{6}\right)n_y^{23} & \frac{1}{2}n_y^{23} \\
\left(\frac{x_3+2x_1}{6}\right)n_x^{31} & \left(\frac{y_3+2y_1}{6}\right)n_x^{31} & \frac{1}{2}n_x^{31} & \left(\frac{x_3+2x_1}{6}\right)n_y^{31} & \left(\frac{y_3+2y_1}{6}\right)n_y^{31} & \frac{1}{2}n_y^{31}
\end{pmatrix}
\begin{pmatrix} a \\ b \\ c \\ d \\ e \\ f \end{pmatrix}
=
\begin{pmatrix} 1 \\ 0 \\ 0 \\ 0 \\ 0 \\ 0 \end{pmatrix}, \tag{52}$$

where we have indicated by (n_x^{lm}, n_x^{lm}), with l and m running locally from 1 to 3, the components of the vector normal to the edge having the lth and the mth nodes as vertices. The Us satisfy the 6×6 linear problem

$$\mathscr{A}U = I, \tag{53}$$

which can be solved directly, giving $U=$ columns of $\mathscr{A}^{-1}$.

With this set of basis functions we must compute the two integrals B and D which appear in equation (23) and the term $BD^{-1}B^{\mathrm{T}}$ which appears in equation (30). Let us define $|\Omega_i|$ as the area of the ith triangle and η_i as the value of the storage on element Ω_i. It is easy to see that

$$D \equiv (d_{ij}) = \int_\Omega S_s \phi_i \phi_j \, \mathrm{d}\Omega = S_s |i| \Omega_i | \delta_{ij} = \eta_i |\Omega_i| \delta_{ij}, \tag{54}$$

$$B \equiv (b_{ij}) = \int_\Omega \nabla \cdot \mathbf{w}_i \phi_j \, \mathrm{d}\Omega = \int_{\Omega_j} \nabla \cdot \mathbf{w}_i \, \mathrm{d}\Omega = \begin{cases} 1 & \text{if } \mathbf{w}_i \neq 0 \text{ on } \Omega_j \text{ (a)}, \\ -1 & \text{if } \mathbf{w}_i \neq 0 \text{ on } \Omega_j \text{ (b)}, \\ 0 & \text{elsewhere.} \end{cases} \tag{55}$$

In case (a) the outward normal to edge e_i has the same orientation as $\mathbf{n}_i$; in case (b) the outward normal has the opposite orientation. Then

$$\begin{aligned} BD^{-1}B^{\mathrm{T}}|_{ij} = & \sum_k \int_{\Omega_k} \nabla \cdot \mathbf{w}_i \, \mathrm{d}\Omega (\eta_k |\Omega_k|)^{-1} \int_{\Omega_k} \nabla \cdot \mathbf{w}_j \, \mathrm{d}\Omega \\ = & \begin{cases} \dfrac{1}{\eta_p |\Omega_p|} + \dfrac{1}{\eta_q |\Omega_q} & \text{if } i=j \text{ and } e_i \text{ is an internal edge}, \\ \dfrac{1}{\eta_p \Omega_p} & \text{if } i=j \text{ and } e_i \text{ is a boundary edge}, \\ -\dfrac{1}{\eta_p \Omega_p} & \text{if } i\neq j \text{ and } \exists \Omega_p \text{ such that } e_i, e_j \in \Gamma_p, \\ 0 & \text{elsewhere}, \end{cases} \end{aligned} \tag{56}$$

where Ω_p and Ω_q—the latter existing only if e_i is not a boundary edge—are the triangles which share the edge e_i and Γ_p is the boundary of the corresponding triangle Ω_p. For the sake of completeness we also present a final useful relation which appeared in our implementation of the algorithm solving equation (30):

$$BB^{\mathrm{T}}|_{ij} = \sum_k \int_{\Omega_k} \nabla \cdot \mathbf{w}_i \, \mathrm{d}\Omega \int_{\Omega_k} \nabla \cdot \mathbf{w}_j \, \mathrm{d}\Omega = \begin{cases} 2 & \text{if } i = j \text{ and } e_i \text{ is an internal edge,} \\ 1 & \text{if } i = j \text{ and } e_i \text{ is a boundary edge,} \\ -1 & \text{if } i \neq j \text{ and } \exists \Omega_p \text{ such that } e_i, e_j \in \Gamma_p, \\ 0 & \text{elsewhere.} \end{cases} \tag{57}$$

2D limiter

Let us denote by C_l^{L} and C_l^{R} respectively the left and right reconstructed values on the lth edge of the mesh of a generic species (the index i has been omitted). Referring to Figure 1, the left value C_l^{L} comes from the reconstruction within the triangle Ω_k and the right value C_l^{R} comes from the reconstruction within the adjacent triangle Ω_{k_e}. The left and the right side of l are defined by the direction of the normal v_l at this edge, which is outwards from the triangle Ω_k and inwards to the triangle Ω_{k_e}. The limiter proposed by Barth [20] is designed in order to ensure that the following two properties are satisfied by the reconstructed values.

(A) The reconstruction must not exceed the minimum and maximum of the neighbouring cell averages.
(B) The difference in the interpolated values at the l the edge, $C_l^{\mathrm{R}} - C_l^{\mathrm{L}}$, and the difference in the corresponding cell averages, $C(\mathbf{x}_k, t) - C(\mathbf{x}_{k_e}, t)$, should have the same sign.

These two properties can be summarized as

$$1 \geq \frac{C_l^{\mathrm{R}} - C_l^{\mathrm{L}}}{C(\mathbf{x}_k, t) - C(\mathbf{x}_{k_e}, t)} \geq 0. \tag{58}$$

To satisfy property (A), Barth [20] showed that it is sufficient to design the limiter as follows.

1. Compute $C_k^{\max}$ and $C_k^{\min}$ as the maximum and minimum of the cell averages in the neighbours of the cell Ω_k.
2. Then a local limiting value ψ_j is introduced for each vertex of the cell Ω_k:

$$\psi_j = \begin{cases} \min\left(1, \dfrac{C_k^{\max} - C_k}{C_j - C_k}\right) & \text{if } C_j - C_k > 0, \\ \min\left(1, \dfrac{C_k^{\min} - C_k}{C_j - C_k}\right) & \text{if } C_j - C_k < 0, \\ 1 & \text{if } C_j - C_k = 0, \end{cases} \tag{59}$$

   where C_j is the extrapolated solution variable at the vertex j.
3. Finally, a global limiting value is estimated as

$$\psi = \min(\psi_1, \psi_2, \psi_3). \tag{60}$$

To satisfy property (B), a check is performed edge-by-edge on the reconstructed values. If these values do not satisfy condition (B), they will be replaced by their mean.

REFERENCES

1. R.W. Harvey, R.L. Smith and L.G. George, 'Effect of organic contamination upon microbial distributions and heterotrophic uptake in a Cape Cod, Mass. aquifer', *Appl. Environ. Microbiol.*, **48**, 1197–1202 (1984).
2. F.H. Chapelle, P.B. McMahon, N.M. Dubrovsky, R.F. Fujii, E.T. Oaksford and D. A. Vroblesky, 'Deducing the distribution of the terminal electron-accepting in hydrologically diverse groundwater systems', *Water Resources Res.*, **31**, 359–371 (1995).
3. D.R. Lovley and F.H. Chapelle, 'Deep subsurface microbial processes', *Rev. Geophys.*, **33**, 365–381 (1995).
4. F.J. Molz, M.A. Widdowson and L.D. Benefield, 'Simulation of microbial growth dynamics coupled to nutrient and oxygen transport in porous media', *Water Resources Res.*, **22**, 1207–1216 (1986).
5. M.A. Widdowson, F.J. Molz and L.D. Benefield, 'A numerical transport model for oxygen- and nitrate-based respiration linked to substrate and nutrient availability in porous media', *Water Resources Res.*, **24**, 1553–1565 (1988).
6. W. Kinzelbach, W. Schafer and J. Herzer, 'Numerical modeling of natural and enhanced denitrification processes in aquifers', *Water Resources Res.*, **27**, 1123–1135 (1991).
7. Y.M. Chen, L.M. Abriola, P.J.J. Alvarez, P.J. Anid and T.M. Vogel, 'Modeling transport and biodegradation of benzene and toluene in sandy aquifer material: comparisons with experimental measurements', *Water Resources Res.*, **28**, 1833–1847 (1992).
8. A. Zysset, F. Stauffer and T. Dracos, 'Modeling of reactive groundwater transport governed biodegradation', *Water Resources Res.*, **30**, 2423–2434 (1994).
9. B.D. Wood, T.R. Ginn and C.N. Dawson, 'Effects of microbial metabolic lag in contaminant transport and biodegradation modeling in a layered porous media system', *Water Resources Res.*, **31**, 553–563 (1995).
10. J.S. Kindred and M.A. Celia, 'Contaminant transport and biodegradation: 2. Conceptual model and test simulations', *Water Resources Res.*, **25**, 1149–1159 (1989).
11. E.O. Frind, W.H.M. Duynisveld, O. Strebel and J. Boettcher, 'Modeling of multicomponent transport with microbial transformation in groundwater: the Furhberg case', *Water Resources Res.*, **26**, 1707–1719 (1990).
12. D.R. Malone, C.M. Kao and R.C. Borden, 'Dissolution and biorestoration of nonaqueous phase hydrocarbons: model development and laboratory evaluation', *Water Resources Res.*, **29**, 2203–2213 (1993).
13. B.D. Wood, C.N. Dawson, J.E. Szecsody and G. Streile, 'Modeling contaminant transport and biodegradation in a layered porous media system', *Water Resources Res.*, **30**, 1833–1845 (1994).
14. J.C. Tracy, L.E. Erikson and L.C. Davis, 'Rate limited degradation of hazardous organic contaminants in the root zone of a soil', *Proc. 86th Annu. Meet. Exhib.*, Denver, CO, June 1993, Air & Waste Management Association, 199X, p. 93-WA-89.02.
15. J.C. Tracy, H. Ramireddy, L.E. Erickson and L.C. Davis, 'Effects of climatological variability on the performance of vegetative systems in remediating contaminated soil', *Proc. 87th Annu. Meet. Exhib.*, Denver, CO, June 1994, Air & Waste Management Association, 199X, p. 94-WA-86.01.
16. C.Y. Chiang, M.F. Wheeler and P.B. Bedient, 'A modified method of characteristics technique and mixed finite elements method for simulation of groundwater solute transport', *Water Resources Res.*, **25**, 1541–1549 (1989).
17. L. Bergamaschi, C. Gallo, G. Manzini, C. Paniconi and M. Putti, 'A mixed finite-elements/TVD finite-volumes scheme for saturated flow and transport in groundwater', in Cecchi *et al.* (eds), *Finite Elements in Fluids*, Padova, 1995, pp. 1223–1232.
18. F. Brezzi and M. Fortin, *Mixed and Hybrid Finite Element Methods*, Springer, Berlin, 1992.
19. C. Hirsch, *Numerical Computation of Internal and External Flows*, Wiley, Chichester, 1990.
20. T.J. Barth, 'Aspects of unstructured grids and finite volume solvers for the Euler and Navier–Stokes equations', in *AGARD Rep. 787*, 1992.
21. R.A. Freeze and J.A. Cherry, *Groundwater*, Prentice-Hall, Englewood Cliffs, NJ, 1979.
22. J.E. Bailey and D.F. Ollis, *Biochemical Engineering Fundamentals*, McGraw-Hill, New York, 1977.
23. F. Brezzi, 'On the existence, uniqueness and approximation of saddle point problems arising from Lagrangian multipliers', *RAIRO Anal. Numer.*, **8**, 129–151 (1974).
24. O. Axelsson, *Iterative Solution Methods*, Cambridge University Press, New York, 1994.
25. L. Bergamaschi, S. Mantica and F. Saleri, 'A mixed finite element approximation of Darcy law in porous media', *Tech. Rep. CRS4-APPMATH-94/20*, 1994.
26. A. Harten, S. Osher, B. Engquist and S.R. Chakravarthy, 'Some results on uniformly high-order accurate essentially nonoscillatory schemes', *Appl. Numer. Math.*, **2**, 347–376 (1986).
27. A. Harten, B. Engquist, S. Osher and S.R. Chakravarthy, 'Uniformly high-order accurate essentially nonoscillatory schemes, III, *J. Comput. Phys.*, **71**, 231–303 (1987).
28. P.K. Sweby, 'High resolution schemes using flux limiters for hyperbolic conservation laws', *SIAM J. Numer. Anal.*, **21**, 995–1011 (1984).

